E-glass/DGEBA/m-PDA Single Fiber Composites: The Effect of Strain Rate on Interfacial Shear Strength Measurements

G. A. HOLMES,* R. C. PETERSON, D. L. HUNSTON,
and W. G. MCDONOUGH

National Institute of Standards and Technology
Polymers Division
Gaithersburg, Maryland 20899-8543

Precise measurements of fiber break regions have been made during the single fiber fragmentation test (SFFT) procedure on E-glass/diglycidyl ether of bisphenol-A (DGEBA)/meta-phenylenediamine (m-PDA) test specimens. From these measurements, the location and size of each fiber fragment was determined, and the resulting information was used to construct fragmentation maps of the tested fiber. By comparing these maps, the fragmentation process supports random fragmentation along the length of the fiber. Since the interfacial shear strength (IFSS) or the interfacial shear stress transfer coefficient (I-STC) is obtained from the fragment length data at the end of the test (saturation), frequency histograms of the fragment length data were constructed to determine the repeatability of the fragmentation process. Since the SFFT is performed by sequential step-strains of the test specimen, test protocols were developed by controlling the step size of each strain increment and the time between each step-strain (dwell time). For the testing protocols used in this research, the E-glass/DGEBA/m-PDA frequency histograms of the fragment lengths were found to be generally repeatable. However, when the effective strain rate of the test was altered by changing the dwell time between strain increments, the fragment distribution at saturation of the E-glass/DGEBA/m-PDA SFFT specimens changed. The direction of the change was found to be inconsistent with the effect one might expect when only the nonlinear viscoelastic behavior of the matrix is considered. However, the magnitude of the change observed in the E-glass/DGEBA/m-PDA SFFT specimens is not universal. Fragmentation data obtained on E-glass/polyisocyanurate SFFT specimens revealed a much smaller change in fragment length distributions with the same change in testing protocols. Consistent with the results obtained on the E-glass/DGEBA/m-PDA, fiber fragmentation occurs when the polyisocyanurate matrix exhibits nonlinear viscoelastic behavior. The implication of these results for interfacial shear strength measurements is discussed.

INTRODUCTION

The development of a reliable microtest method that measures fiber-matrix interface strength in composite materials has been the focus of numerous research efforts. This research has been driven by the recognition that the interface or interphase in many composite materials has a profound effect on the onset of failure (e.g., off-axis properties in unidirectional composites and the shear strength of composite laminates). In composites, internal failure of the constituent materials generally precedes macroscopic failure. The internal failure modes of composite materials that may be observed are (a) fiber fracture, (b) micro-cracking of the matrix, (c) fiber-matrix de-bonding, and (d) delamination (1). The strength and toughness (damage tolerance) of the interface or interphase are important considerations in all these failure modes.

Since composites are used in structural applications, the resistance of the fiber-matrix interface to environmental attack is also of concern. Hence, reliable and accurate data on the fiber-matrix interface is essential for predicting the long-term performance of a composite structure. Microtests are used to isolate fiber-matrix interface effects from other complex effects

*To whom correspondence should be addressed.

that arise when testing full-scale composites and to investigate in a systematic manner the effect of fiber-fiber interactions on interface or interphase performance. In addition, full-scale composites are often expensive to test. Thus, the development of a microtest that accurately assesses interface strength and durability is desirable. Of the current microtests, the single fiber fragmentation test (SFFT) is well-suited for durability experiments since the fiber is completely embedded (similar to fibers in full-scale composites), the fiber is loaded in a manner similar to a full-scale composite, and the specimen can be totally immersed in the fluid of choice. After exposure, the SFFT specimen is tested in the normal manner to assess changes in the interfacial shear strength.

In the SFFT, a dog bone is made with a high extension-to-failure resin and a single fiber embedded along the axis of the dog bone. The sample is pulled in tension by applying sequential step-strains of approximately 1.1 s in duration and 15 μm in length. Changing the time between step-strains (dwell time) alters the test time and the "effective" strain rate of the test. By straining the matrix, the stress is transmitted into the fiber through the fiber-matrix interface. Since the fiber has a lower strain-to-failure than the resin, the fiber breaks at the weakest flaw as the strain is increased. The fiber fragmentation process continues until the resulting fiber fragments are all shorter than a critical transfer length (l_c). The critical transfer length is defined as the length below which the fragments are too short for sufficient load to be transmitted into them to cause additional failure. This point is termed saturation. The lengths of the fragments at saturation are measured, and a micromechanics model [e.g., Cox (2) or Kelly-Tyson (3)] is used to convert the average fragment length into a measure of the interface stress transfer coefficient (I-STC). Hence, the I-STC, which has been loosely related to the interface strength, is determined indirectly from experimental data and micromechanics models. The success of this approach in characterizing the interface or interphase clearly depends on the accuracy of the micromechanics model. With existing models, this test correctly orders the change in model composites interface strength, where the bonding character of the fiber-matrix interface or interphase region has been systematically altered by the use of bonding and nonbonding silane coupling agents (4). However, intercomparisons of interface strength when the matrix properties are allowed to change (e.g., by changing the matrix system or by exposing the matrix to moisture) have not been universally successful. Although I-STC values obtained from laser Raman spectroscopy (LRS) appear to be less dependent on model assumptions (5), this technique is only suitable for certain fibers. Hence, for the carbon (e.g., AS-4) and glass fibers typically used in composite materials, LRS is not useful.

To overcome these shortcomings and increase our understanding of the fiber-matrix interface or interphase stress transfer process, researchers have advocated the development of realistic micromechanics models (6). Central to the development of these new models are the assumptions typically used in their derivations. These assumptions are (a) the matrix material is linear elastic or elastic-perfectly plastic and (b) a perfect bond exists between the fiber and the matrix. Two additional limitations have also been noted in the development of new models. These are (a) the radius of matrix parameter, r_m, used in Cox-type models is undefined (7, 8) and (b) yielding of the matrix is not considered. In addition, as noted by Shioya *et al.* (9), these models make no assumption about the failure process occurring at the interface or interphase region.

Recently, more attention has been directed toward addressing the validity of the above assumptions. Research using LRS has shown that r_m is typically between 2 and 10 times the diameter of the fiber (5,10–12). These results now allow for r_m to be redefined in terms of a cylindrical element around the fiber beyond which the matrix extends freely under the influence of the applied strain (5). This definition implies that the I-STC, provided r_m can be determined independently, is a material parameter (i.e., independent of test specimen size). In addition, the inappropriateness of the elastic-perfectly plastic matrix assumption has been established for many polymer matrices by LRS. Feillard *et al.* (13) showed by numerical modeling that predictions of the number of fiber breaks in an epoxy based SFFT test specimen are best done by utilizing a secant modulus-based Cox model, rather than the elastic modulus-based Cox model. Recent work in our laboratory (14, 15) has shown that the diglycidyl ether of bisphenol-A (DGEBA) metaphenylenediamine (m-PDA) matrix typically used to assess the I-STC exhibits nonlinear viscoelastic behavior above 1% strain. Moreover, fragmentation of the embedded E-glass fiber occurs primarily in the nonlinear viscoelastic region of the stress-strain curve. These observations have also been shown to be true when an E-glass fiber is embedded in a polyisocyanurate network (16). Hence, determining the I-STC from current micromechanics models becomes problematic, since the Cox and Kelly-Tyson models assume linear elastic and elastic-perfectly plastic matrix behavior, respectively. At saturation, the actual stress in the DGEBA/m-PDA matrix is intermediate between the response predicted by the linear elastic modulus used in the Cox model and the elastic-perfectly plastic assumption used in the Kelly-Tyson model (see *Fig. 1*). To account for this deviation from assumption 1, the Cox model was extended to the nonlinear viscoelastic regime by utilizing the *Elastic-Viscoelastic Correspondence Principle* and *Schapery's Correspondence Principle* (17). Therefore, for an elastic fiber embedded in a nonlinear viscoelastic matrix, the shear-stress transfer process in the new model depends on the stress-strain and time-dependent behaviors of the matrix.

Relative to the nonlinear model, the elastic-based Cox model over-predicts the I-STC by a fraction of ap-

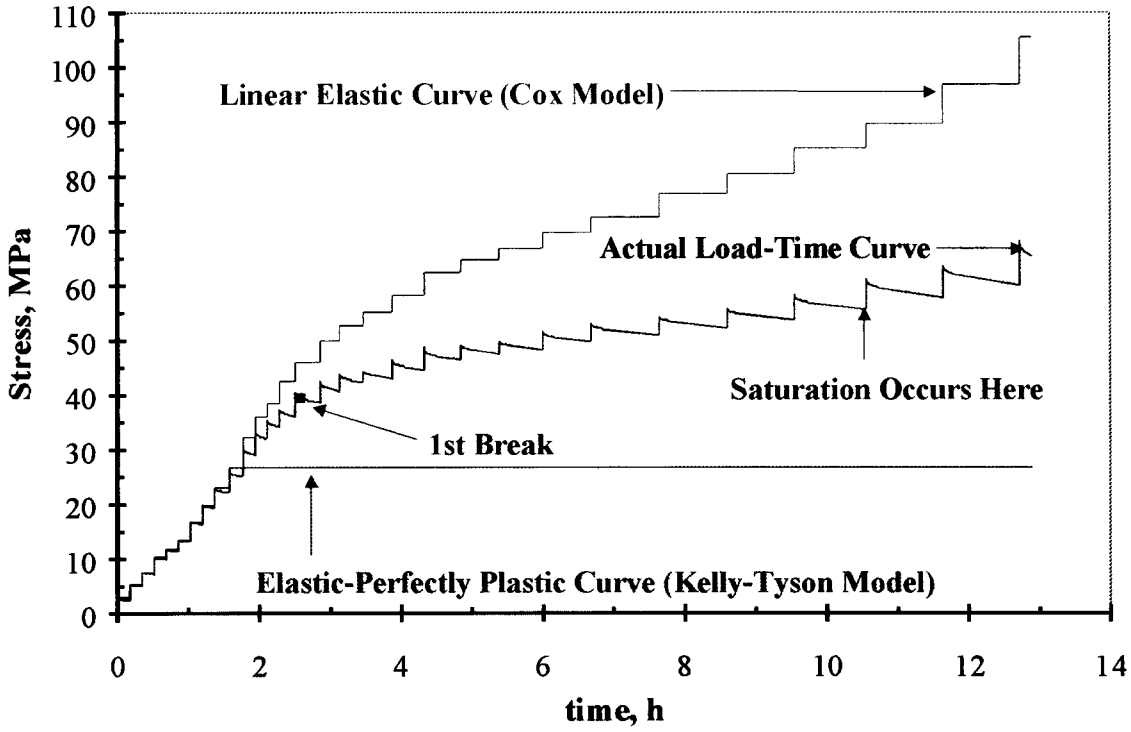

Fig. 1. Typical stress-time curve for E-glass/DGEBA/m-PDA single fiber composite.

proximately 20%. This result is consistent with the numerical simulations of Feillard *et al.* (13). Additional evidence supporting the importance of the matrix in the fragmentation process is the occurrence of fracture events at times considerably longer (>10 min) than the application time of a step-strain (≅1.1 s). These delayed fracture events are inconsistent with elastic and elastic-perfectly plastic matrix behavior, and the occurrence of these events has led some researchers to suggest a specified protocol for performing the test. This suggests that the number of breaks at saturation, and hence the I-STC, depends on the test protocol. In addition, it has been suggested that high matrix strains may exist in the region between fiber breaks. Depending on the stress-strain behavior of the matrix, these regions could significantly perturb the stress field at the fiber ends and promote interface failure. We will look critically at the effect of strain rate on the final fragment length distribution, since the mean of the final fragment length distribution is a key parameter in determining the I-STC. Therefore, significant changes in the final fragment length distribution can indicate significant changes in the I-STC. To minimize factors that must be considered at the fiber-matrix interface or interphase, bare E-glass fibers were used in all of the specimens tested. In a subsequent paper, debond region formation and debond region strain in these specimens will be investigated. Since the DGEBA/m-PDA matrix is nonlinear viscoelastic, the effect of strain rate on debond region formation will also be investigated in the second paper. In the third paper, we will examine the relationship of the results of this paper and the second paper with matrix material behavior during the fragmentation process. Since determining the I-STC is dependent on the fragment length distribution at saturation, it is appropriate that the initial paper in this series focus on this aspect.

EXPERIMENTAL

Fiber and Mold Preparation

To make single fiber fragmentation specimens, eight-cavity molds were prepared with RTV-664 from General Electric (18) following the procedure described by Drzal (19). All molds were post-cured at 150°C and rinsed with acetone prior to use. A 30.48 cm (12 inch) long tow of fibers was cut from a spool of E-glass (from Owens-Corning). The fibers were shown previously to be bare (i.e., no processing aids or sizings). The tow was washed with spectrophotometric grade acetone and vacuum dried at 100°C overnight before cooling prior to use. Single filaments of E-glass fiber were separated from the 30.48 cm tow, and care was taken to touch only the ends of the fiber. The central portion of a fiber was aligned down the central axis of each mold cavity with the aid of sprue slots. The fibers were temporarily fixed in place by pressing them onto double-stick tape. Small strips of double-stick tape were placed over each fiber end to hold them in place until permanently mounted with 5-min epoxy.

Embedding Procedure

One hundred grams of diglycidyl ether of bisphenol-A (DGEBA, Epon 828 from Shell Chemical Co.) and 14.5 g of meta-phenylenediamine (m-PDA, Fluka Chemical Company) were weighed out in separate beakers. To lower the viscosity of the resin and melt the m-PDA crystals, both beakers were placed in a vacuum oven (Fisher Scientific Isotemp Vacuum Oven, model 281 A) set at 75°C. After the m-PDA crystals were completely melted, the silicone molds containing the fibers were placed into another oven (Blue M Stabiltherm, model OV-12A) that was preheated to 100°C. The preheated oven was turned off and the molds allowed to heat for approximately 20 min. This last procedure dries the molds and minimizes the formation of air bubbles during the curing process.

At approximately 9 min before the preheated molds were removed from the oven, the m-PDA was poured into the DGEBA and thoroughly mixed. The mixture was placed into the vacuum oven and degassed for approximately 7 min. After removing the preheated molds from the oven, the mold cavities were filled with the DGEBA/m-PDA resin mixture using 10 cc disposable syringes. The filled molds were then placed into a programmable oven (Blue M, General Signal, model MP-256-1, GOP). A cure cycle of 2 h at 75°C followed by 2 h at 125°C was used.

Fragmentation Test

The fiber fragmentation tests were carried out on a small hand-operated loading frame, similar to that described by Drzal (19), mounted on a Nikon Optiphot polarizing microscope. Before loading the specimen, the cross section dimensions of the gauge section were measured using a Mitutayo electronic digital caliper. The maximum uncertainty in these measurements is ± 0.005 mm. After mounting the specimen, the image was viewed using a CCD camera (Optronics LX-450 RGB Remote-Head microscope camera) and monitor (Sony, PVM-1344Q). Before the test, the fiber diameter was measured with an optical micrometer (VIA-100 from Boeckeler) attached to the video system. Nineteen measurements of the fiber diameter were taken along the fiber length. The standard deviation in these measurements is typically ± 0.31 μm. The sample was scanned by translating the loading frame under the microscope with a micrometer. The position of the load frame was monitored by a Linear Variable Differential Transducer (LVDT) (Trans-Tek, Inc. model 1002-0012) connected to an Analog-to-Digital board (Strawberry Tree, Inc.) in a computer. To measure fragment lengths or other points of interest in the sample, the location was aligned with a cross hair in the microscope as seen on the video monitor, and the position of the LVDT was digitized into the computer. The standard instrumental uncertainty in measuring a point is ± 0.3 μm. However, the standard uncertainty in reproducibly relocating a point is ± 1.1 μm. Using propagation of error (20), the relative combined standard uncertainty of the global strain values reported in *Figs. 3* and *10–13* is 0.023%. The combined standard uncertainty of the fragment lengths used in *Figs. 4–7* and *12–15* is 1.6 μm.

The load was monitored during the experiment using a 2,224 N (500 pound) load cell connected to a bridge (load cell and AED 9001A bridge, Cooper Instruments). The standard uncertainty in the stress measurements shown in *Fig. 1* is ± 3% of the stress. The bridge was attached to the same computer via a serial connection. A customized program was developed to continuously record the load and any LVDT measurements made. The average application time of each strain-step performed in *Fig. 1* was (1.10 ± 0.17) s and the average deformation was (14.45 ± 3.11) μm, where the uncertainties cited represent one standard error.

Since the loading frame is not infinitely stiff, relaxation of the stress with time resulted in an increase in specimen strain with time. The compliance of the instrument was determined to be 0.0034% for each 1 N change in load. Therefore, for relaxations depicted in *Fig. 1*, the strain increase in each time interval is less than 0.0005. Thus, the increase in strain due to stress relaxation is insignificant.

Data Analysis

Analysis of variance (ANOVA) statistics are used primarily to detect changes between fragment length distributions generated by the single fiber fragmentation test. However, the fragmentation data are presented in histogram form. To minimize the subjectivity involved in histogram construction and facilitate graphical comparisons, an optimal bin size (~75 μm) for the histograms shown in *Figs. 4–6* was obtained by averaging estimates from three methods specifically developed to calculate optimal histogram bin size (21–24). The data from these calculations are shown in *Tables 1* and *2*, along with the summary statistics for the specimens tested.

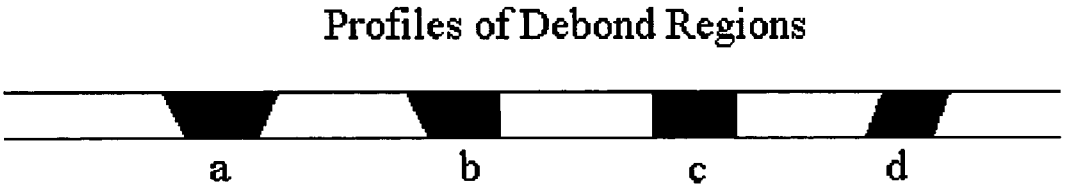

Fig. 2. Profiles of common debond regions.

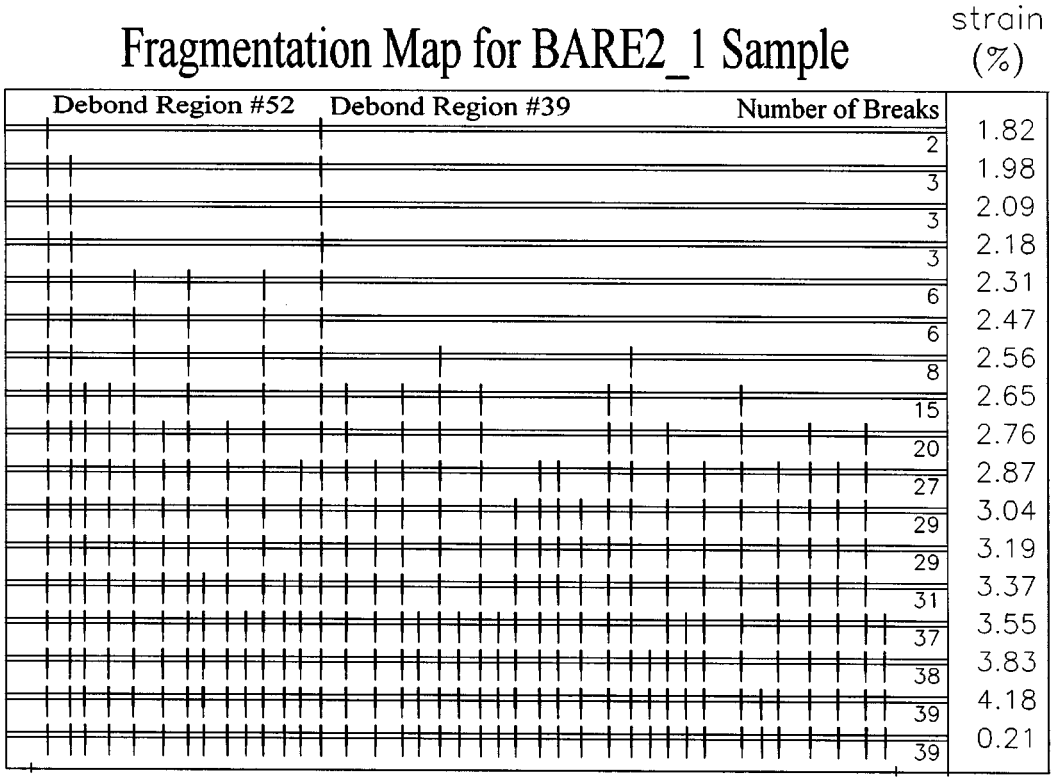

Fig. 3. A typical fragmentation map for bare E-glass/DGEBA/m-PDA SFFT specimens.

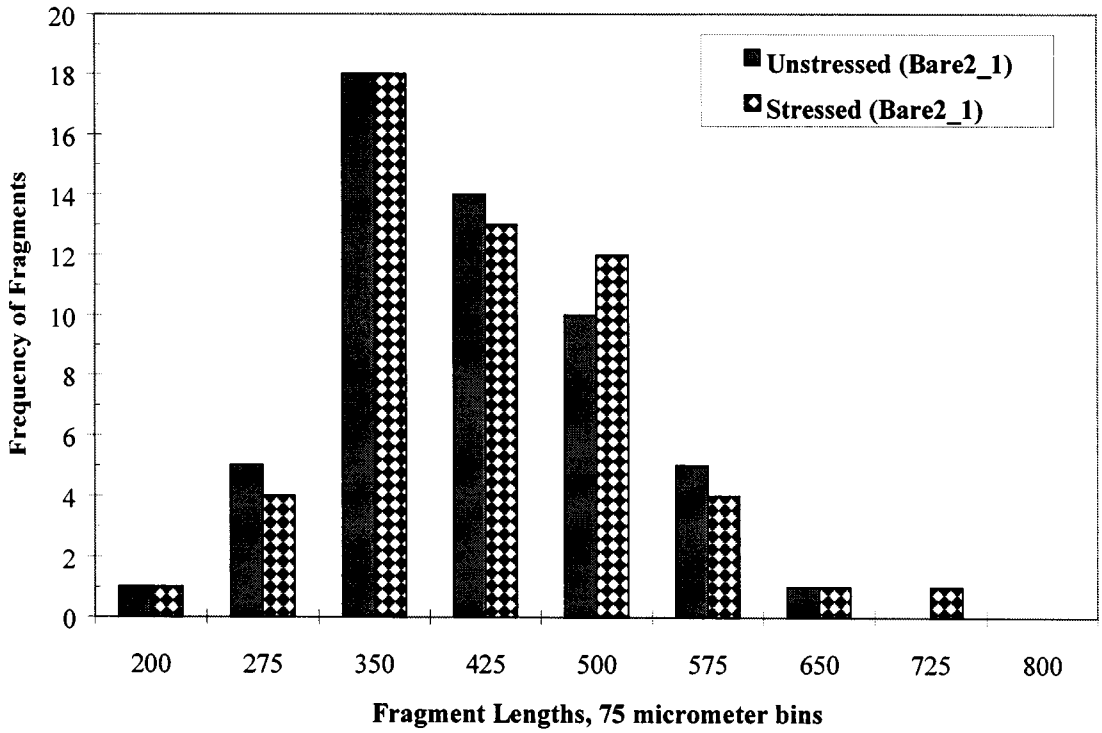

Fig. 4. Histograms of Bare2_1 SFFT test specimen in the stressed and unstressed states.

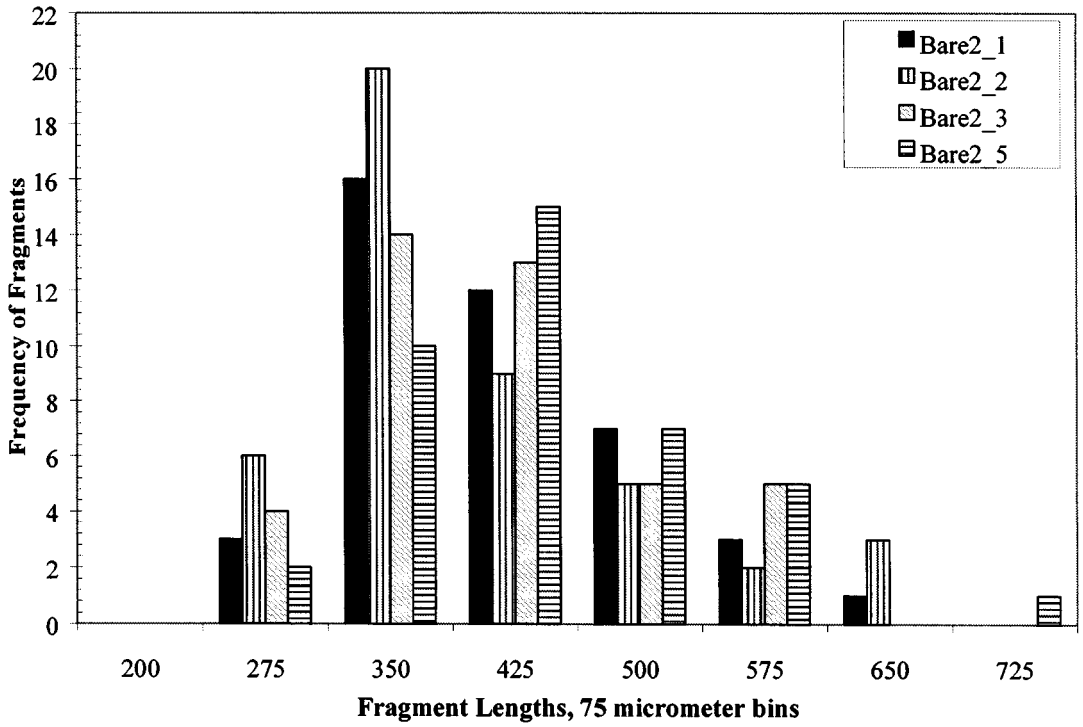

Fig. 5. Histograms for E-glass/DGEBA/m-PDA SFFT specimens tested using variable test protocol (intermediate test rate).

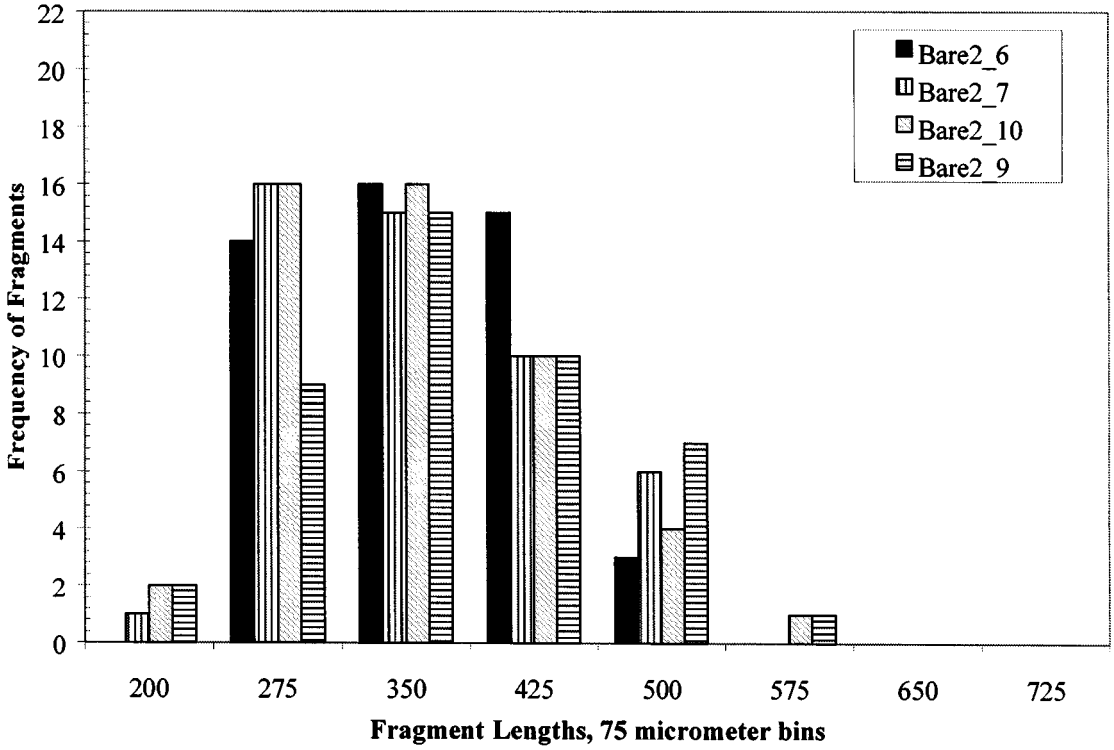

Fig. 6. Histograms for E-glass/DGEBA/m-PDA SFFT specimens tested using 1 h between strain increment test protocol (slow test rate).

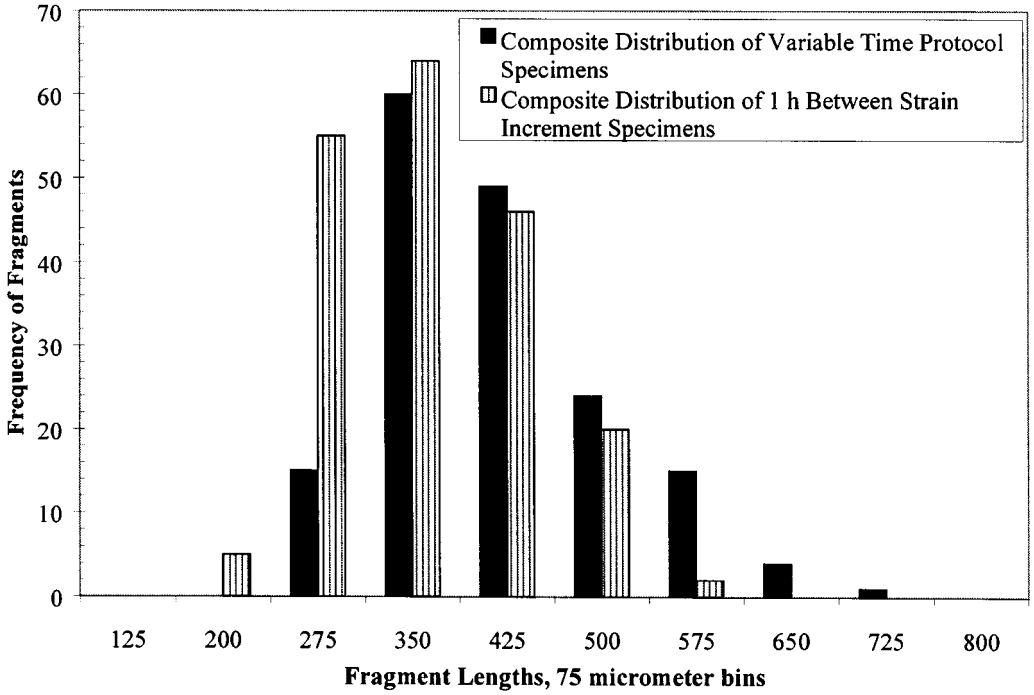

Fig. 7. Aggregated histograms of variable time protocol specimens and 1 h between strain increment protocol specimens.

Table 1. Summary Statistics and Optimum Bin Calculation for Fragments from Intermediate Strain Rate Fracture Specimens.

Distribution Statistics/Samples	Bare2_1	Bare2_2	Bare2_3	Bare2_5	
Mean, μm	378.9	359.4	377.6	404.3	
Standard Deviation, μm	86.7	98.9	88.8	85.5	
Median, μm	367.8	341.2	363.0	394.3	
Maximum Value, μm	644.2	593.8	561.2	684.4	
Minimum Value, μm	242.0	228.0	206.3	262.1	
Upper Quartile, Q3, μm	429.9	424.6	431.9	449.1	
Lower Quartile, Q1, μm	314.2	283.4	317.6	341.8	
Interquartile Range (IQR), μm	115.7	141.1	114.3	107.2	
Binning Method					**Average**
Scott (1979)	87.1	96.8	89.9	87.2	90.3
Freedman and Diaconis (1981a)	64.3	71.9	66.2	64.1	66.6
Freedman and Diaconis (1981b)	66.6	79.4	66.3	62.7	69.9
	Overall Average				**75.2**

Table 2. Summary Statistics and Optimum Bin Calculation for Fragments from Slow Strain Rate Fracture Specimens.

Distribution Statistics/Samples	Bare2_6	Bare2_7	Bare2_9	Bare2_10	
Mean, μm	321.6	320.7	343.0	316.4	
Standard Deviation, μm	74.8	74.6	83.9	80.1	
Median, μm	310.5	304.3	337.9	307.5	
Maximum Value,μm	452.0	496.5	507.6	522.5	
Minimum Value, μm	205.1	181.2	195.9	176.1	
Upper Quartile, Q3, μm	390.8	371.5	410.6	359.5	
Lower Quartile, Q1, μm	255.4	262.5	277.3	252.4	
Interquartile Range (IQR), μm	135.4	109.1	133.3	107.1	
Binning Method					**Average**
Scott (1979)	71.8	71.6	83.0	75.4	75.5
Freedman and Diaconis (1981a)	53.7	53.5	61.5	56.6	56.3
Freedman and Diaconis (1981b)	74.5	60.0	75.5	57.8	66.9
	Overall Average				**66.2**

RESULTS AND DISCUSSION

General Observations During Fiber Fracture

During fragmentation experiments on bare E-glass/DGEBA/m-PDA SFFT specimens, darkened regions (between (15 to 30) μm) form at each fiber break site. Reconstructions of the typical break regions are shown in *Fig. 2*. The light-to-dark region interface in the fiber break region is taken by the authors to be bonding and complete debonding areas at the fiber-matrix interface, respectively. The bonded region may include interface material damaged during fiber fragmentation but not completely debonded from the fiber. By damage it is meant that the adhesion at the fiber-matrix interface has been altered from its original state at the start of the test by breaking some of the chemical or physical bonds at the interface. Profile "a" is the most often observed debond region followed by "b" and "c". Profiles "a" and "d" are characterized by taking four measurements at the corners of the darkened region. Similarly, profiles "b" and "c" require three and two measurements, respectively. Across the fiber diameter, ≅ 15 μm, the location of the darkened region differs on average in profiles "a" and "b" by approximately 3 μm. Interestingly, these break regions decreased in length without a change in shape when the applied strain was removed after saturation was reached. This length change is used to deduce the strain in these break regions and will be discussed in detail in the next paper.

A Fortran program was written to study the fiber break pattern and to estimate the global strain in the test specimen. The program reads in a file that contains the break locations and debond regions after each step-strain. In addition, the program uses the gauge lengths prior to loading and at a point where there are two or more breaks in the fiber. The latter is taken as a starting point, and the program calculates the strain at this point based on the gauge length measurements. The location of each fiber break is noted, and where debond regions are present, the centroid of the debond region is used to estimate the break location. The program then moves to the data obtained after the next step-strain and finds the break locations. The breaks present in both data sets are identified and the break locations at the higher strain are shifted and scaled to get the best agreement with the corresponding break locations at the lower strain. The shift provides a measure of the relative change in strain. This process is repeated with each new step-strain being matched to the shifted and scaled values before the step-strain. Once saturation is reached, the results are plotted as shown in *Fig. 3*. These plots provide a fragmentation map that illustrates the fiber break pattern and how it develops with strain. The shift information is then combined with the starting point strain determined from the gauge length measurements to estimate the absolute strain after each step. If these values are compared with the strains found from direct measurement of the gauge length, the two agree to within the significant digits reported for percent strain in *Fig. 3*. Data from several fragmentation maps were examined and no consistent pattern to the fragmentation processes was found, consonant with the assumption that the fragmentation process along the fiber length is random.

After saturation, the strain was released from the SFFT specimen. As noted above, the break regions shrink in length when the applied strain is removed. After allowing for a 24 h recovery period, the break region locations were remeasured in the unstressed state. The residual strain in the unstressed state is approximately 0.2% (see *Fig. 3* - the last strain increment). In *Fig. 4*, histograms of a SFFT specimen at saturation in the stressed and unstressed state are shown. The distributions differ slightly, reflecting the increased length of the fragments in the stressed state.

Effect of Strain Rate on Fiber Distribution

For these tests, nine bare E-glass fiber test specimens, denoted by Bare2_x and Bare3_x, were used. The 'Bare2' and 'Bare3' labels refer to the second and third batches made of these specimens, respectively. The 'x' denotes the specimen number from a given batch. During the testing procedure, Bare2_4 fractured before saturation was reached. A test was initiated on the Bare2_8 specimen, but was halted prematurely. Since the Bare2_8 specimen had been loaded to above 1.0% strain, it was not reloaded and subjected to further testing.

Four specimens were tested using a variable test protocol (described below), and four specimens were tested using a 1 h between strain increment test protocol (slow test rate). The final specimen was tested using a 10 min between strain increment test protocol (fast test rate). In *Fig. 5*, the fragment distribution from four SFFT specimens are shown. These specimens were loaded at 10 min pauses between strain increments until the occurrence of the first break. The dwell time between subsequent strain increments was increased to the time required to measure all of the breaks. Since the number of breaks increases with strain, the dwell time at a given strain depends on the number of breaks, hence the name variable test protocol (intermediate test rate). The total test times, the number of fragments, and the calibrated gauge lengths for each specimen are given in *Table 3*. A typical example of the variable test protocol is the stress-time loading curve shown in *Fig. 1*.

For specimens Bare2_1 to Bare2_3, the maximum number of fiber fragments occurs in the (275 to 350) μm class interval. In *Fig. 5*, the (275 to 350) μm class interval is denoted by the 350 μm label on the x-axis. These specimens exhibit a single common mode at 312.5 μm. The distributions of all three specimens are similar with the average fragment lengths and standard deviations being (379 ± 87) μm, (359 ± 99) μm, and (378 ± 89) μm, respectively. The average fragment length for Bare2_5 is (404 ± 85) μm. Although the maximum frequency of fiber breaks for the

Table 3. Associated statistics for Histograms Given in *Figs. 5, 6, 14* and *15*.

Sample	Protocol	Total Test Time, h	Number of Fragments	Sampling Length, mm
Bare3_1	10 Min	5.5	44	16.34
Bare2_1	Variable	13	42	16.12
Bare2_2	Variable	12	45	16.31
Bare2_3	Variable	13	41	15.89
Bare2_5	Variable	14	40	16.35
Bare2_6	1 h	25	48	15.74
Bare2_7	1 h	28	48	15.79
Bare2_9	1 h	29	44	15.95
Bare2_10	1 h	32	49	15.85
PUO4E01	10 min	6	48	15.49
PUO4E02	Variable	15	48	15.48
PUO4E03	1 h	36	50	15.31

Bare2_5 specimen occurs in the (350 to 425) μm class interval, single factor ANOVA statistics indicate that this distribution is indistinguishable at the 95% confidence level (p-value (25) > 0.05) from the Bare2_1 to Bare2_3 fiber length distributions (p-value = 0.1584). Even though Bare2_5 is statistically indistinguishable from specimens Bare2_1 to Bare2_3, this p-value is significantly decreased from the p-value obtained when only Bare2_1 to Bare2_3 are compared (p-value = 0.5400). The summary statistics for these data are given in *Table 1*.

In *Fig. 6*, the histograms of four specimens tested using the 1 h between strain increment test protocol (slow test protocol) are shown. For the Bare2_6, 7, and 10 SFFT specimens, the maximum number of fiber fragments are split, almost evenly, between the (200 to 275) and (275 to 350) μm class intervals. In contrast to the variable test protocol specimens discussed above, these specimens exhibit a broad mode. Statistically these three distributions are equivalent with a p-value of 0.937. Including specimen Bare2_9 decreases the p-value for equivalence of the four specimens to 0.318. Thus, Bare2_9 is statistically equivalent at the 95% confidence level to specimens Bare2_6,7,and 10. However, the decrease in p-value with the inclusion of Bare2_9 might indicate a trend toward a significant difference from the other 3 populations. This behavior is similar to the behavior noted when Bare2_5 was included with specimens Bare2_1 to Bare2_3. The summary statistics for the slow protocol data are given in *Table 2*. The total test times, the number of fragments, and the calibrated gauge length for the slow protocol specimens are given in *Table 3*.

The major differences between the two (variable and slow protocol test) data sets are the number of fragments in the class intervals found between (125 to 275) μm and (500 to 725) μm. This is best seen from the aggregated histograms shown in *Fig. 7*. Even though the optimum bin size (class interval) for the aggregated histogram is approximately 45 μm, the 75 μm bin size is used in this histogram construction to facilitate comparison with *Figs. 5* and *6* histograms. In *Fig. 7*, the 1 h between strain increment specimens have 4 times more fragments than the variable time protocol specimens in the class intervals found between (125 to 275) μm, while the variable time specimens have 20 times more fragments in the class intervals found between (500 to 725) μm than the slow protocol specimens. As a result, the mean of the fragment length distribution from the slow protocol test specimens [(325 ± 79) μm] is lower by a fractor of 14.3% relative to the mean of the fragment length distribution from the variable time specimens [(379 ± 91) μm]. Statistically, the difference between the two aggregated data sets is significant (p-value = 3.39E-09).

Summary statistics for the aggregated histograms in *Fig. 7* are shown in *Table 4* (strain = saturation). Of immediate interest in this table are the skewness and the kurtosis of the variable and slow protocol fragment length distributions at saturation. The skewness measures the deviation from symmetry of a distribution, and the kurtosis measures the peakedness of a distribution (i.e., is the center, or peak, much shorter or taller than that of a normal distribution?). Normality (gaussianity) of the distribution is typically rejected if the ratio of either statistic to its standard error is less than −2 or greater than +2 (26). For the aggregated histogram of the intermediate test protocol specimens, the fragment length distribution exhibits positive skew-

Table 4. Summary Statistics for Aggregated Histograms in *Figs. 7, 12* and *13*.

Distribution Statistics/Samples	Protocol			
	Variable	Slow	Variable	Slow
Strain	Saturation	Saturation	2.55%	2.45%
Mean, μm	379.4	325.3	641.5	526.7
Standard Deviation, μm	90.9	78.5	432.5	217.9
Median, μm	365.2	315.2	507.8	473.5
Maximum Value, μm	684.4	522.5	3026.5	1709.7
Minimum Value, μm	206.3	176.1	233.3	249.1
Upper Quartile, Q3, μm	431.9	390.0		
Lower Quartile, Q1, μm	308.9	262.9		
Interquartile Range (IQR), μm	123.0	127.1		
Skewness	0.690	0.336	3.062	1.823
Standard Error of Skewness	0.187	0.175	0.240	0.217
Kurtosis	0.183	–0.719	11.656	6.177
Standard Error of Kurtosis	0.379	0.349	0.476	0.430

ness (skewness/std. error = 0.690/0.187 = 3.69). Recalling that Bare2_5 exhibited a higher mode value than Bare2_1 to 3 (see *Fig. 5*), analysis excluding the Bare2_5 specimen also indicates positive skewness (skewness/std. error = 3.36). In contrast, the skewness ratio for the aggregated histogram of the slow test protocol specimens is only 1.92. The slightly low negative kurtosis ratio (kurtosis/std. error = −0.719/0.349 = −2.06) exhibited by the slow test protocol aggregated histogram results from including the Bare2_9 specimen, which exhibits a higher mode value than the other slow test protocol specimens (see *Fig. 6*). Excluding the Bare2_9 specimen changes the kurtosis and skewness ratios to 1.60 and 1.98, respectively. The kurtosis in the aggregated histogram of the intermediate test protocol specimens is only 0.49. Therefore, slow test protocol specimens yield fragment distributions within the limits of normality, whereas the fragment distributions from intermediate test protocol specimens exhibit positive skewness.

Neter *et al.* (27) state that the F test for the equality of factor level means is little affected by lack of normality, either in terms of level of significance or power of the test. Therefore, the ANOVA result for the aggregated distributions discussed above is valid, since non-normality in the distributions is minimal.

Since the mean of the fragment length distribution, $<l>$, is used to calculate the critical transfer length, l_c, via the theoretical equation $l_c = (4/3) <l>$, it is of interest to determine if these two distributions yield fragments only between $l_c/2$ and l_c. These limits arise from the Kelly-Tyson equation (3, 28). Using l_c calculated from the average of the fragment distributions, both aggregated specimens have a fraction of approximately (4 to 5)% of the fragments below $l_c/2$ and a fraction of approximately 10% of the fragments above l_c. For the slow and intermediate aggregated specimens, the fragments below $l_c/2$ are within 41 μm and 47 μm of the lower limit, respectively. Fragments in the slow test protocol specimens exceed l_c, the upper limit, by no more that 90 μm, while fragments from the intermediate test protocol specimens exceed the high limit by no more than 180 μm. Recalling that Bare2_5 and Bare2_9 exhibited different modal behavior, excluding these specimens from the analysis resulted in l_c for the aggregate of the slow and intermediate test protocol specimens being exceeded by no more than 96 μm and 148 μm, respectively. This difference in exceeded range at the upper limit is consistent with the positive skewness exhibited by the intermediate test protocol specimens. For this restricted analysis, the fragments below $l_c/2$ are within 37 μm and 42 μm of the lower limit, respectively. Thus, neither test protocol yields fragment distributions conforming to the theoretical limits dictated by the Kelly-Tyson equation. Even though the slow test protocol specimens do not exhibit gross deviations from normality by the skewness and kurtosis criteria, both aggregate distributions exhibit some positive skewness. This positive skewness remains even when Bare2_5 and Bare2_9 are excluded (see *Fig. 8*). It should be noted that the optimum bin size (class interval) of 50 μm was used in *Fig. 8* to more clearly show the positive skewness in the aggregate histogram of the slow

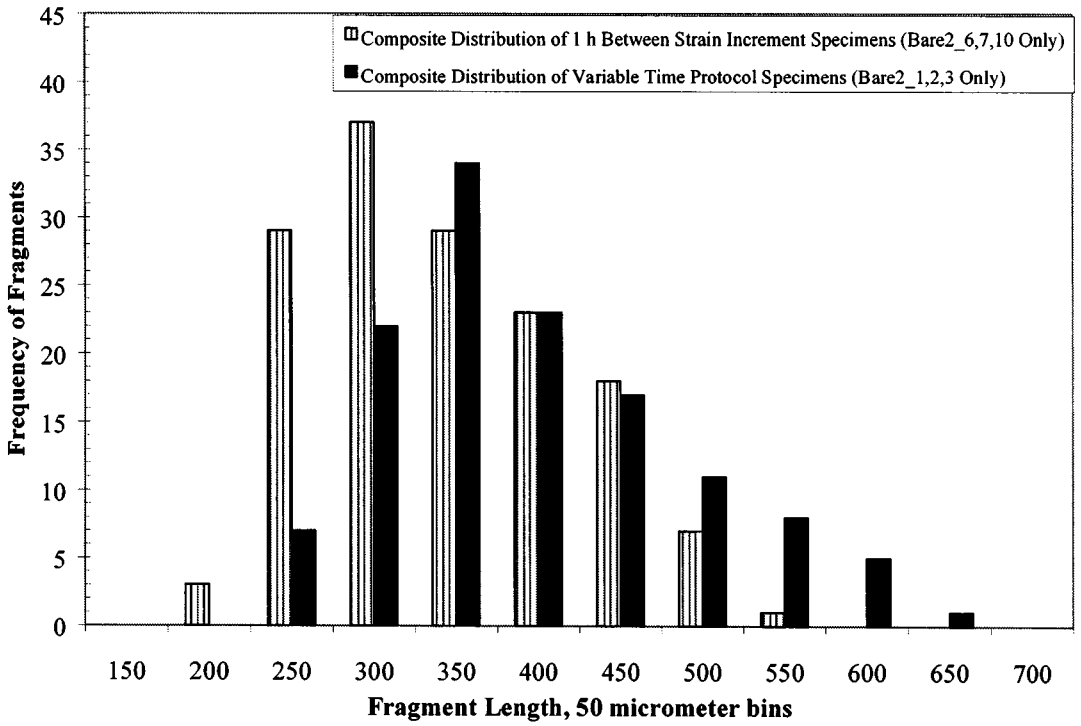

Fig. 8. Aggregated histograms of variable time protocol specimens (excluding Bare2_5) and 1 h between strain increment protocol specimens (excluding Bare2_9).

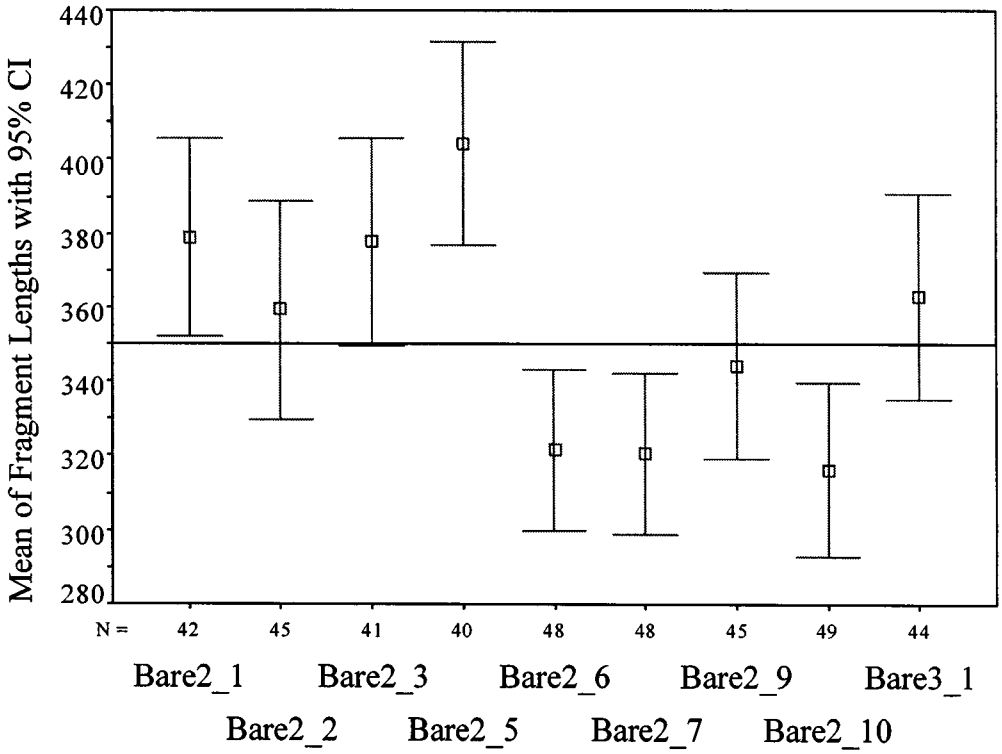

Fig. 9. Mean plot of unstressed fragment lengths with 95% confidence intervals. Bare2_1 to Bare2_5 are intermediate fracture rate specimens. Bare2_6 to Bare2_10 are slow fracture rate specimens. Bare3_1 is a fast fracture rate specimen.

test protocol specimens. This deviation from the ideal limits may be due in part to damage of the intact interface near the fiber ends and changes in the matrix stiffness with increasing strain, since the matrix influences the critical transfer length. The stiffness of this matrix as measured by the secant modulus has been shown previously to decrease by a fraction of 55% during the SFFT experiment (14, 17).

Since the mean value of the fragment length distribution is used to calculate the I-STC, the means of all specimens are plotted with 95% confidence intervals in *Fig. 9*. The mean values in this figure indicate an increased variability in the means when specimens are tested by the intermediate test protocol. The intermediate test protocol and fast specimens have higher mean values, giving a lower value of the I-STC. Since the variable and slow test protocol specimens came from the same batch, this suggests that the difference in means, and hence changes in I-STC, is due to changes in the testing protocol.

Evolution of Fiber Breaks

Plots of the number of fiber breaks versus strain are often used to monitor the evolving fragmentation process and detect saturation. Two such plots for the fragments tested by the intermediate and slow test protocols are shown in *Figs. 10* and *11*. In monitoring the test specimen for saturation, the number of breaks in the uniform cross-section of the dog bone is used. Hence, the number of breaks shown in these two plots are greater than the breaks taken from the calibrated gauge section length. For the intermediate protocol test specimens in *Fig. 10*, the number of fiber breaks in the gauge section at approximately 2.54 % strain ranges from 30 to 44. For the slow test protocol test specimens shown in *Fig. 11*, the number of fiber breaks in the gauge section at (2.4 to 2.5) % strain ranges from 38 to 48. At this point in the fragmentation process there appears to be a distinction between the two test protocols with respect to the evolving break pattern. By taking the stressed fragment lengths from the calibrated gauge sections for the strains denoted by open symbols in *Fig. 10* and closed symbols in *Fig. 11*, aggregated histograms were constructed for the intermediate (variable) test protocol specimens and the slow (1 h between strain increments) test protocol specimens. These histograms are shown in *Figs. 12* and *13*, respectively. The summary statistics for the two aggregated histograms are also given in *Table 4*. Since these distributions are nonnormal, quartile values in *Table 4* were not calculated.

At saturation, a 10 μm shift in the class interval position is required to minimize the shift of fragments between class intervals (see *Fig. 4*) and keep the stressed distribution consistent with the unstressed distribution. Thus, at approximately 2.5 % strain a

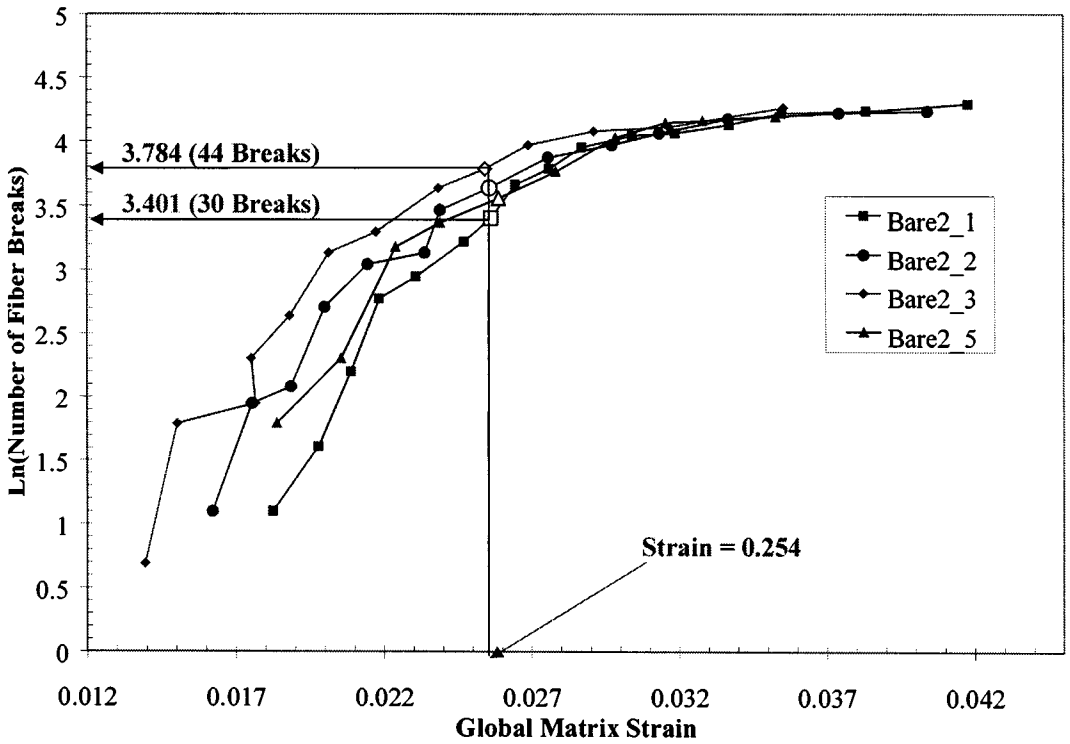

Fig. 10. Number of fiber breaks versus strain for the variable test protocol specimens (complete gauge length used).

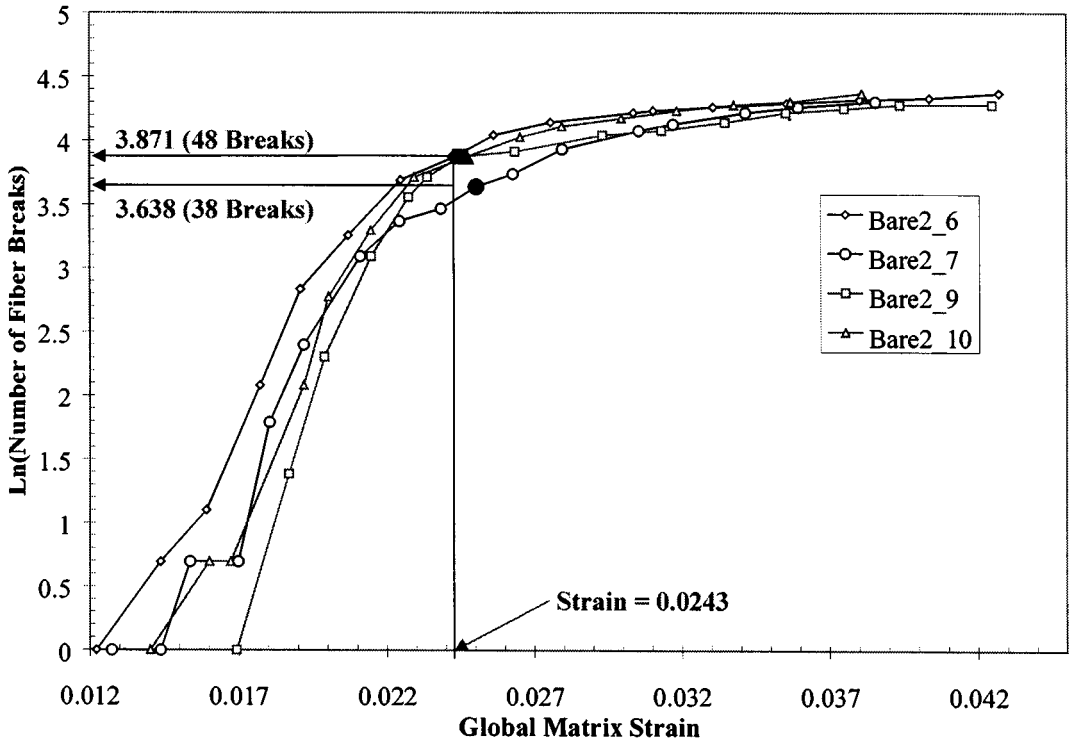

Fig. 11. Number of fiber breaks versus strain for the slow test protocol specimens (complete gauge length used).

5 μm shift in the class interval location in *Figs. 12* and *13* has been used to facilitate comparison with the unstressed aggregated histograms in *Fig. 7*. Comparing *Figs. 12* and *13*, it is clear that the major differences between the two distributions are the relative number of stressed fragments found in the (280 to 355) μm

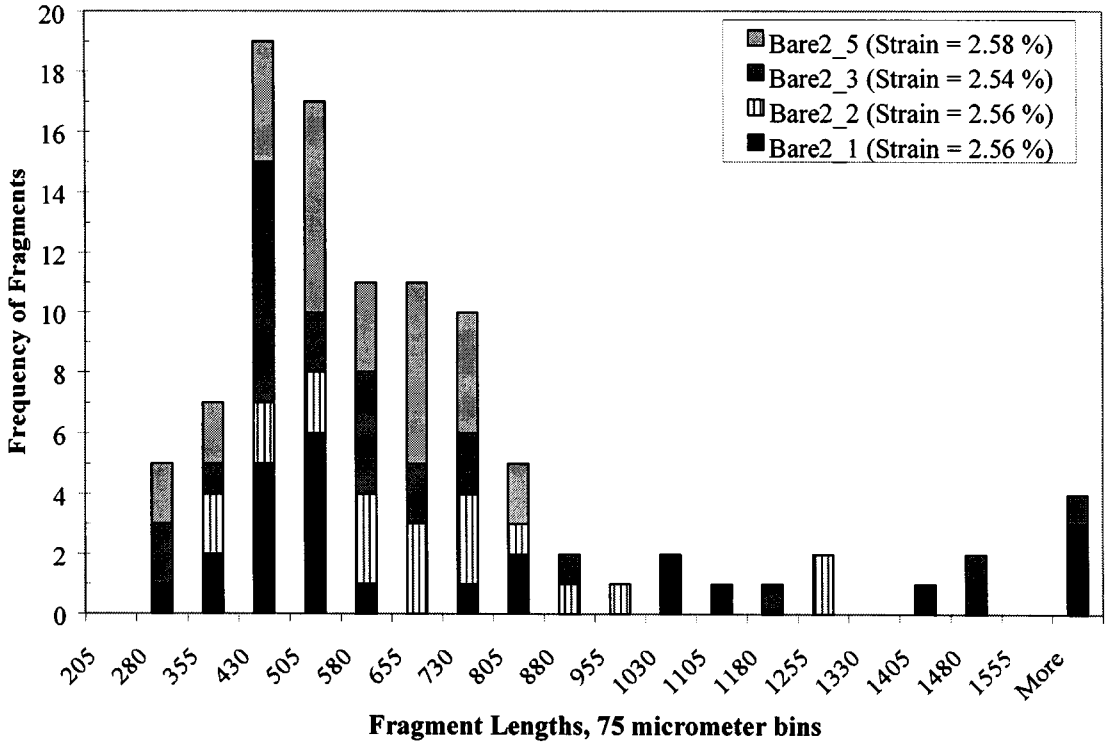

Fig. 12. Histogram of variable time protocol specimens at approximately 2.55% strain.

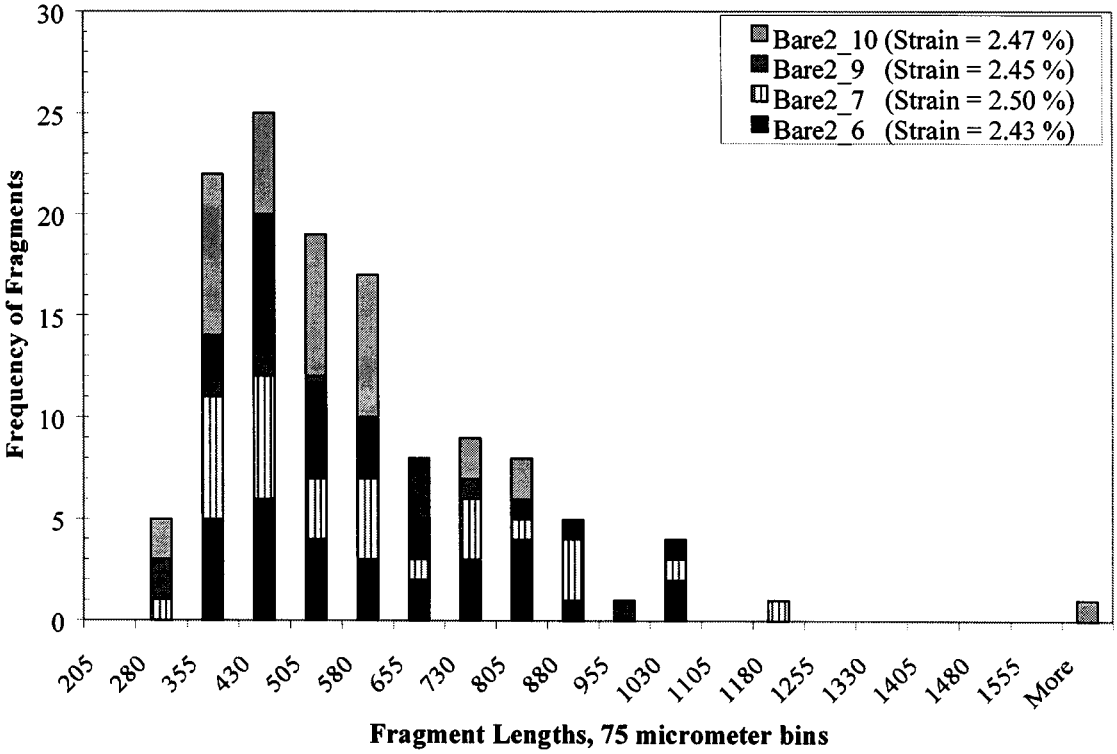

Fig. 13. Histogram of 1 h between strain increment protocol specimens at approximately 2.45% strain.

and (355 to 430) μm class intervals and the almost complete absence of stressed fragments above 1180 μm in the slow protocol test specimens (*Fig. 13*). To compare the fragment length distributions in *Figs. 12* and *13* with the saturated fragment length distributions in *Fig. 7*, the number of class interval fragments

for the distributions at 2.5% strain was subtracted from the corresponding class interval fragments at saturation. These values are found in *Table 5*. Although both data sets at 2.5% strain have the same number of fragments in the (205 to 280) μm class interval, during the latter stage of the tests five times more fragments are formed in this class interval, (200 to 275) μm, in the slow protocol test specimens than in the intermediate test protocol specimens. This suggests that the critical transfer length in the slow protocol test specimens is on average smaller than in the intermediate protocol tests specimens during the latter stages of the test.

To determine if the differences in the two distributions at 2.5% strain are significant, ANOVA is used. It is evident from *Figs. 12* and *13* that the two aggregated distribution are not normal. For the distributions shown in *Figs. 12* and *13*, the non-normality as characterized by the skewness and kurtosis are given in *Table 4*. For distributions that exhibit extreme non-normality, the samples are often logarithmically transformed before statistical analyses are done (26). The kurtosis ratio (kurtosis/std. error) and skewness ratio (skewness/std. error) in "ln" space for the slow protocol fragment distribution at 2.5% strain are 0.091 and 2.13, respectively. For the intermediate protocol fragmentation distribution at 2.5% strain these values are 3.489 and 4.45, respectively. For the ANOVA of the two distributions shown in *Figs. 12* and *13* in "ln" space, the p-value for significance is 0.021. Based on this test, the differences noted above in *Figs. 12* and *13* are significant. In addition, the mean fragment length for the aggregate of the slow test protocol specimens at 2.5% strain is 100 μm smaller than the mean fragment length for the aggregate of the intermediate test protocol specimens (see *Table 4*). These results suggest that up to 2.5% strain, the critical transfer length in the slow test protocol specimens is on average shorter than specimens tested by the intermediate test protocol. From these calculations, the cause of the difference in the final fragment length distributions shown in *Fig. 7* appears to occur at strain values lower than 2.45%.

Test For Time-Related Contributions

The total test time for the slow test protocol is typically twice as long as the variable test protocol (see *Table 3*). Hence, it is possible that test time, in addition to the effective loading rate, may contribute to the larger number of breaks and smaller fragments exhibited in the slow test protocol specimens. To investigate this possibility, two approaches were used. For specimens tested using the intermediate test protocol, these specimens were taken to saturation and allowed to remain for several days at elevated strains to determine if additional breaks would occur after saturation was achieved. No additional breaks were found.

Additional tests were performed using SFFT specimens made with bare E-glass fibers embedded in a polyisocyanurate network. These specimens were then tested using the fast, variable, and slow test protocols used on the bare E-glass/DGEBA/m-PDA SFFT specimens. The fragment distributions are virtually unaffected by the loading protocol (see *Fig. 14*). These distributions are indistinguishable at the 95% confidence level (p-value = 0.349). Representative data sets from the E-glass/DGEBA/m-PDA SFFT specimens are shown in *Fig. 15* for comparison. In contrast, these distributions are distinguishable at the 95% confidence level (p-value = 0.048). These results indicate that the sensitivity of E-glass/DGEBA/m-PDA SFFT specimens to testing protocol is associated with the matrix and the fiber-matrix interface. The total test time, the number of fragments, and the calibrated gauge length for specimen shown in these figures are given in *Table 3*.

CONCLUSIONS

Data from fragmentation maps support the randomness of the fragmentation process along the length of the fiber. For the E-glass/DGEBA/m-PDA SFFT specimens investigated here, increasing the time between strain increments results in smaller fragments and a higher interfacial shear strength. This result is in contrast to what is predicted based solely on viscoelastic considerations. At the current time, no definitive ex-

Table 5. Numerical Data from Aggregated Histograms in *Figs. 7, 12* and *13*.

Class Interval	Protocol		Class Interval	Protocol		Fragments Formed After 2.5 %	
Saturated	Variable	Slow	2.5%	Variable	Slow	Variable	Slow
125-200	0	5	130-205	0	0	0	5
200-275	15	55	205-280	5	5	10	50
275-350	60	64	280-355	7	22	53	42
350-425	49	46	355-430	19	25	30	21
425-500	24	20	430-505	17	19	7	1
500-575	15	2	505-580	11	17	4	–15
575-650	4	0	580-655	11	8	–7	–8
650-725	1	0	655-730	10	9	–9	–9
725-800	0	0	730-805	5	8	–5	–8
Over 800	0	0	Over 805	16	12	–16	–12

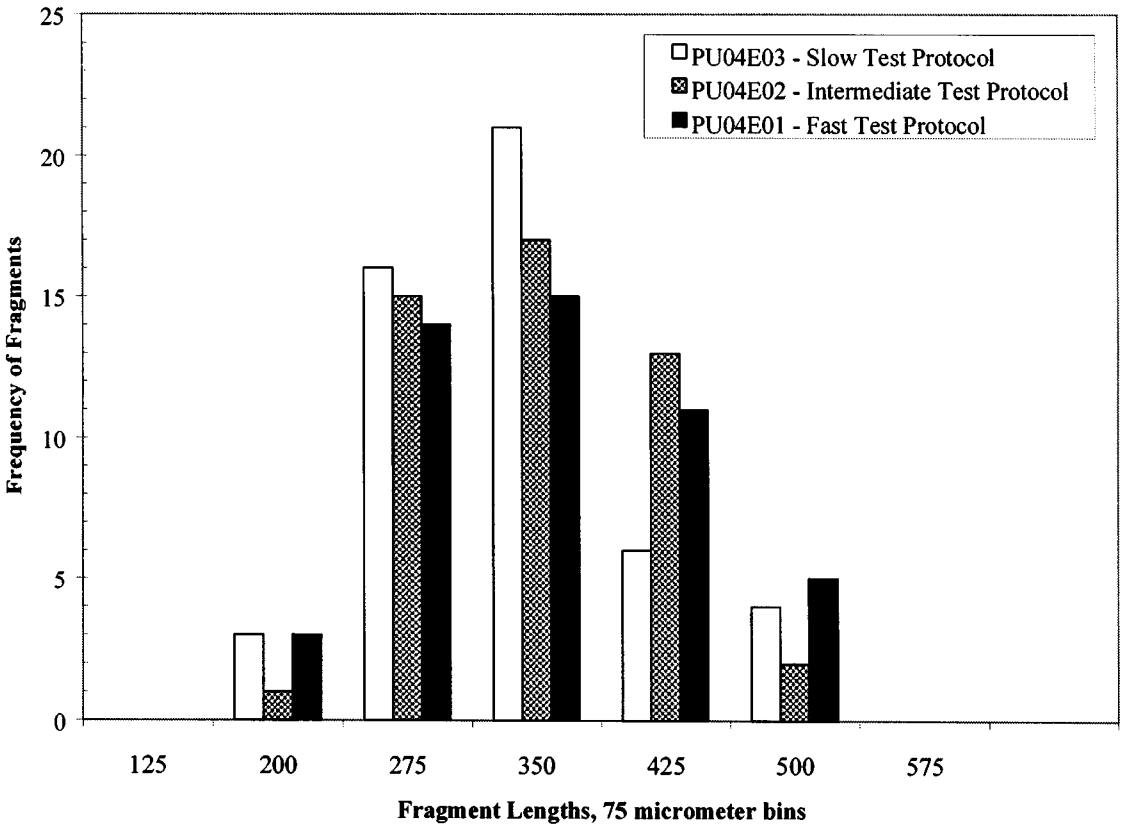

Fig. 14. Effect of test protocol on bare E-glass/polyisocyanurate SFFT specimens.

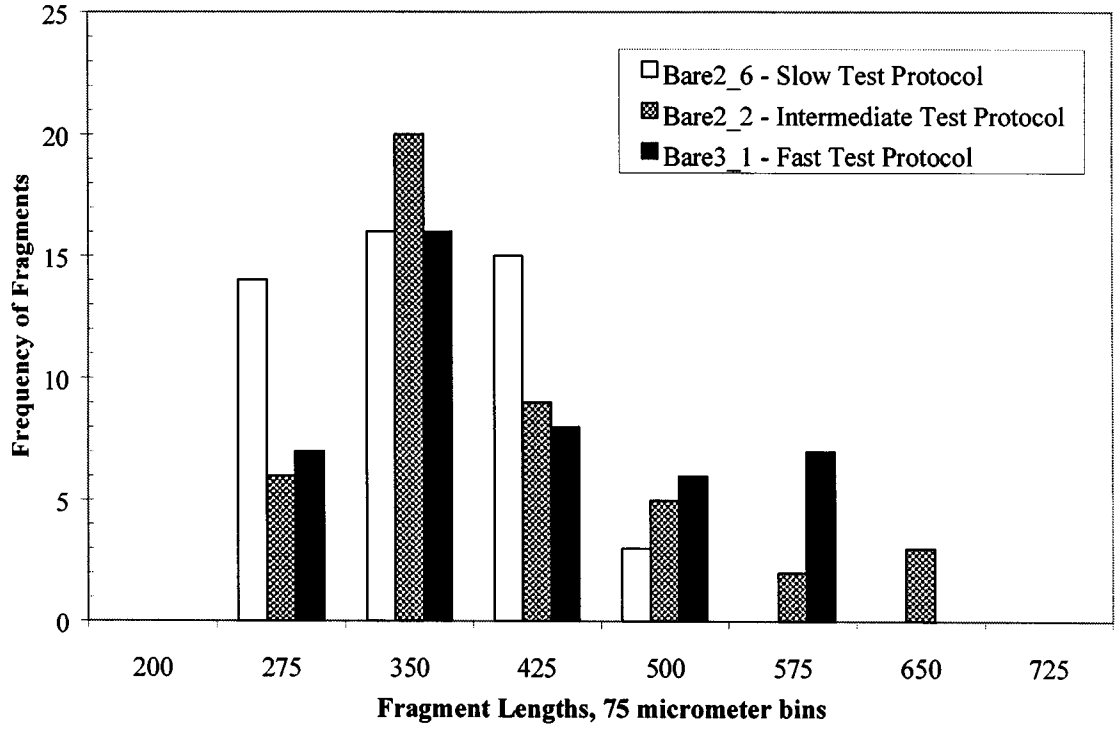

Fig. 15. Effect of test protocol on bare E-glass/DGEBA/m-PDA SFFT specimens.

planation has been advanced to explain this behavior. However, two avenues are being pursued which may be different aspects of the same mechanism. The first assumes that differences in the post yield behavior of the matrix may result from changes in the dwell time between step-strains. A second approach assumes that fiber-matrix interface failure may be occurring during the test. Support for the latter assumption can be found in the work of Carrara and McGarry (29). These researchers found that Cox-type models underpredict the maximum shear stress at the fiber ends by a fraction of approximately 50% when compared to results obtained from finite element analysis. Carrara and McGarry showed that the Cox approximation is reasonable at regions far from the fiber end, but that the radial deformation lines bend sharply near the fiber ends and can only be crudely represented by straight lines. Hence, Cox-type models effectively disregard stress concentration effects at the fiber ends. Recent investigations by Jahankhani and Galiotis (30) using laser Raman spectroscopy revealed that stress concentrations at the fiber ends can result in premature failure of the fiber-matrix interface and a reduction in the I-STC. They also found, when large stress concentrations exist at the fiber ends, that the Cox model fits the shear profile at the fiber ends if the r_m parameter in the Cox model is reduced by a factor of three relative to the r_m value needed when the stress concentrations at the fiber ends are minimal.

Applying the above results to the current research suggests that increasing the dwell time between strain increments allows additional time for stress at the fiber-matrix interface to relax and keep the interface stresses below the value necessary to initiate failure. Since the behavior exhibited by the E-glass/DGEBA/m-PDA SFFT specimens is not universal, more research is needed to completely understand the problem. However, the results presented here indicate clearly that test protocols should be specified when reporting I-STC values.

ACKNOWLEDGMENTS

The authors would like to thank Stefan D. Leigh and Cindy L. Clark for their careful proofing of this manuscript.

REFERENCES

1. B. D. Agarwal and L. J. Broutman, *Analysis and Performance of Fiber Composites*, 2nd Ed., p. 87, John Wiley & Sons, New York (1990).
2. H. L. Cox, *Brit. J. Appl. Phys.*, **3**, 72 (1952).
3. A. Kelly and W. R. Tyson, *J. Mech. Phys. Solids*, **13**, 329 (1965).
4. D. L. Hunston, K. Macturk, C. Schultheisz, G. A. Holmes, W. G. McDonough, and C. L. Schutte, *European Adhes. Conf.*, Vol. 2, pp. 427-432, Inst. of Mater., Cambridge, England (Sept. 1996).
5. C. Galiotis, *Compos. Sci. Technol.*, **42**, 125 (1991).
6. W. G. McDonough, G. A. Holmes, D. L. Hunston, and R. S. Parnas, *NISTIR 6102* (1997).
7. In the original derivation of the Cox model, the radius of the matrix (r_m) parameter was defined as the interfiber distance. Since there is no adjacent fiber in a SFFT specimen this parameter has often been taken as half the thickness of the sample specimen (8). This effectively makes the I-STC dependent on the specimen size.
8. El. M. Asloun, M. Nardin, and J. Schultz, *J. Mater. Sci.*, **24**, 1835 (1989).
9. M. Shioya, W. G. McDonough, C. L. Schutte, and D. L. Hunston, *Proc. 17th Ann. Mtg.*, Adhes. Soc., Orlando (1994).
10. Z. F. Li and D. T. Grubb, *J. Mater. Sci.*, **29**, 189 (1994).
11. N. Melanitis, C. Galiotis, P. L. Tetlow, and C. K. L. Davies, *J. Mater. Sci.*, **28**, 1648 (1993).
12. N. Melanitis, C. Galiotis, P. L. Tetlow, and C. K. L. Davies, *Composites*, **24**, 459 (1993).
13. P. Feillard, G. Desarmot, and J. P. Favre, *Compos. Sci. Technol.*, **49**, 109 (1993).
14. G. A. Holmes, R. C. Peterson, D. L. Hunston, and W. G. McDonough, *Proc. 21st Ann. Mtg.*, p. 175, R. A. Dickie, ed., Adhes. Soc., Savannah (1998).
15. G. A. Holmes, R. C. Peterson, and D. L. Hunston, *Proc. 2nd Int. Conf. Mech. Time-Dependent Mater.*, p. 26 , SEM-Center for Time Dependent Materials, Pasadena, Calif. (1998).
16. W. G. McDonough, G. A. Holmes, and R. C. Peterson, *Proc. 13th Tech. Conf. Compos. Mater.*, pp. 1688-1699, Am. Soc. for Compos., Baltimore (Sept. 1998).
17. G. A. Holmes, R. C. Peterson, D. L. Hunston, W. G. McDonough, and C. L. Schutte, "The Effect of Nonlinear Viscoelasticity on Interfacial Shear Strength Measurements," in *Time Dependent and Nonlinear Effects in Polymers and Composites*, ASTM STP 1357, R. A. Schapery, ed., p. 98, ASTM (2000).
18. Certain commercial materials and equipment are identified in this paper to specify adequately the experimental procedure. In no case does such identification imply recommendation or endorsement by the National Institute of Standards and Technology, nor does it imply necessarily that the product is the best available for the purpose.
19. L. T. Drzal and P. J. Herera-Franco, "Composite Fiber-Matrix Bond Test," in *Engineered Materials Handbook: Adhesives and Sealants*, p. 391, ASM Int., Metals Park, Ohio (1990).
20. H. H. Ku, *J. Res. Natl. Bur. Stand. (U.S.) - C. Engr. and Instr.*, **70C**, 332 (1966).
21. D. W. Scott, *Biometrika*, **66**, 605 (1979).
22. D. Freedman and P. Diaconis, *Z. Wahrsch. V. Gebiete*, **57**, 453 (1981).
23. D. Freedman and P. Diaconis, *Z. Wahrsch. V. Gebiete*, **58**, 139 (1981).
24. D. C. Hoaglin, F. Mosteller, and J. W. Tukey, *Understanding Robust and Exploratory Data Analysis*, p. 25, John Wiley & Sons, New York (1983).
25. R. L. Ott, *An Introduction to Statistical Methods and Data Analysis*, 4th Ed., p. 230, Duxbury Press, Belmont, Calif. (1993).
26. *SPSS Base 8.0 Applications Guide*, pp. 27-28, SPSS Inc., Chicago (1998).
27. J. Neter, M. H. Kutner, C. J. Nachtsheim, and W. Wasserman, *Applied Linear Statistical Models*, 4th Ed., p.776, Irwin, Chicago (1996).
28. R. B. Henstenburg and S. L. Phoenix, *Polym. Comp.*, **10**, 389 (1989).
29. A. S. Carrara and F. J. McGarry, *J. Comp. Mater.*, **2**, 222 (1968).
30. H. Jahankhani and C. Galiotis, *J. Comp. Mater.*, **25**, 609 (1991).